Chapter 6

The Cascading and Doubling Algorithm: Application to Periodic Waveguide Gratings

6.1 Gratings

Although periodically stratified media have been a subject of study and discussion since 1887 [76], the interest in corrugated dielectric waveguides initially started with the possibility of guiding light by dielectric layers. Corrugated waveguides, also called gratings, have since been playing important roles in the design and operation of many devices in integrated optics. Figure 6.1 shows a typical example of a waveguide with rectangular corrugations. There are a variety of applications of

gratings in integrated optics. The most common of these applications is in wavelength filtering. In addition, gratings are used in coupling the electromagnetic field into and out of integrated optical waveguides and devices [77, 78]. This application relies on electromagnetic coupling through phase matching of the different fields by the corrugated region.

6.2 Classification of Gratings

Gratings are widely used as components for realizing wavelength dispersion, conversion, modulation and control of guided wavefronts in optical integrated circuits [79]. Gratings have dimensions, structures and fabrication processes that are suitable for integration. Gratings are also applied as both active and passive device components. Distributed Feedback (DFB) [80] and Distributed Bragg Reflector (DBR) lasers [81, 82] are examples of corrugation-based active devices. In reference [83], some examples of passive grating components are presented which includes grating couplers, deflectors, reflectors, mode converters, wavelength filters and wavelength lenses.

6.3 Analysis of Gratings

A number of theoretical methods have been reported for the analysis of waveguides with periodic corrugations. Marcuse [43] used coupled-mode theory to analyze a

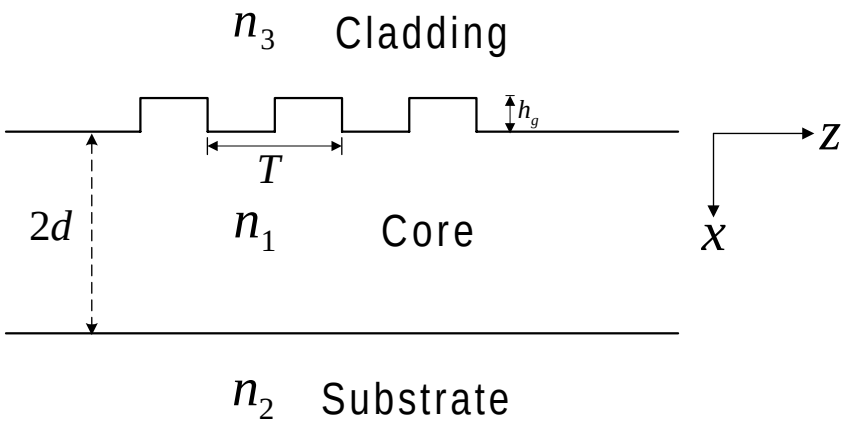

Figure 6.1: Corrugated Waveguide

slab waveguide with sinusoidal deformation on one of its interfaces. The spectral response of a grating filter using coupled-mode theory was calculated and compared with experimental work in [84]. In reference [85], the Effective-Index method was used to model a waveguide grating and the results were compared with coupled-mode theory. A major limitation of the coupled-mode theory is that it can only model small waveguide perturbations which is due to its approximate formulation. The Method of Lines is suited to model such problems, where waveguide perturbations can be large, as it does not have any approximation except for the approximation of the second-derivative operator using central-difference formula. In order to model a long grating with deep corrugations, a fast and stable algorithm within the Method of Lines framework has been developed. This method, named Cascading and Doubling Algorithm [38] can model gratings with thousands of periods much more efficiently than the layer-by-layer algorithm given in chapter 4. In the current chapter, the derivation of this algorithm is explained and comparisons are made with published

results.

6.4 The Cascading and Doubling Algorithm

With reference to figure 6.2, two distributed discontinuities 'A' and 'B' are brought together and are separated by a uniform region of width d. The quantities R_{A1}, T_{A2} (R_{A2}, T_{A1}) are respectively the reflection and transmission matrices of discontinuity 'A' when the field is incident from left(right) of the discontinuity. The individual reflection and transmission matrices of both discontinuities are assumed to be known. We will next develop a scheme to find the reflection and transmission matrices of the combined structure. R_A and T_A are reflection and transmission matrices of the isolated structure 'A'. For an asymmterical discontinuity $R_{A1} \neq R_{A2}$ and $T_{A1} \neq T_{A2}$. The same comments apply to discontinuity 'B'. If the two discontinuities are not identical then $R_A \neq R_B$ and $T_A \neq T_B$. The reflection and transmission matrices of the combined structure are denoted by R_0 and T_0 respectively. These matrices are obtained by adding the successive reflections and transmissions of the incident field as the two structures interact with each other. The field propagation in the uniform waveguide section of length 'd' is described by $e^{\pm jSz}$. The field vector a_0 is assumed to be incident from the left on the first discontinuity (see figure 6.3). We can express the net reflected field in terms of the summation of forward and backwards traveling waves after multiple reflections from the two discontinuities, which gives:

$$R_{01}a_0 = R_{A1}a_0 + T_{A1}e^{jSd}R_{B1}e^{jSd}T_{A2}a_0 + T_{A1}\left(e^{jSd}R_{B1}e^{jSd}R_{A2}\right)e^{jSd}R_{B1}e^{jSd}T_{A2}a_0 +$$

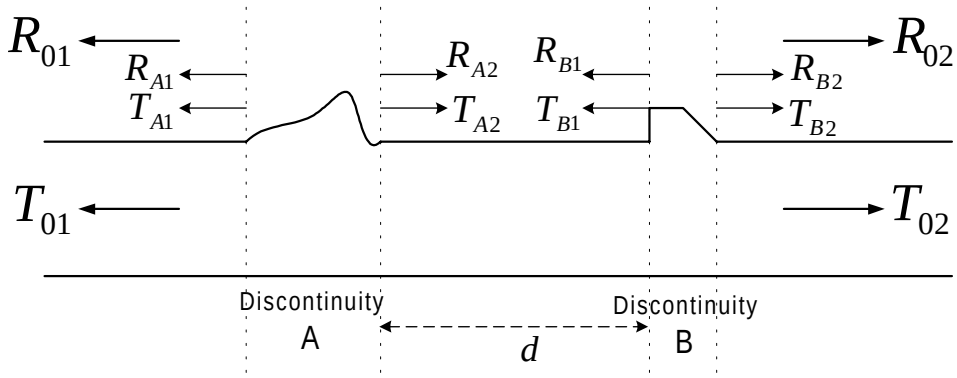

Figure 6.2: Two Waveguide Structures Cascaded Together

$$T_{A1}\left(e^{jSd}R_{B1}e^{jSd}R_{A2}\right)^2 e^{jSd}R_{B1}e^{jSd}T_{A2}a_0 +$$

$$T_{A1}(e^{jSd}R_{B1}e^{jSd}R_{A2})^3 e^{jSd}R_{B1}e^{jSd}T_{A2}a_0 + ... \tag{6.1}$$

$$R_{01}a_0 = R_{A1}a_0 + T_{A1}\left[\sum_{n=0}^{\infty}\left(e^{jSd}R_{B1}e^{jSd}R_{A2}\right)^n\right]e^{jSd}R_{B1}e^{jSd}T_{A2}a_0 \tag{6.2}$$

$$R_{01} = R_{A1} + T_{A1}\left[\sum_{n=0}^{\infty}\left(e^{jSd}R_{B1}e^{jSd}R_{A2}\right)^n\right]e^{jSd}R_{B1}e^{jSd}T_{A2} \tag{6.3}$$

$$R_{01} = R_{A1} + T_{A1}\left(I - e^{jSd}R_{B1}e^{jSd}R_{A2}\right)^{-1}e^{jSd}R_{B1}e^{jSd}T_{A2} \tag{6.4}$$

where the infinite geometric series in 6.3 is assumed to be convergent and is replaced by an equivalent quotient term. The transmission matrix T_0 of the combined structure is obtained in a similar fashion.

$$T_{02}a_0 = T_{B2}e^{jSd}T_{A2}a_0 + T_{B2}\left(e^{jSd}R_{A2}e^{jSd}R_{B1}\right)a_0 +$$

$$T_{B2}\left(e^{jSd}R_{A2}e^{jSd}R_{B1}\right)^2 e^{jSd}T_{A2}a_0 + ... \tag{6.5}$$

$$T_{02}a_0 = T_{B2}\left[\sum_{n=0}^{\infty}\left(e^{jSd}R_{A2}e^{jSd}R_{B1}\right)^n\right]e^{jSd}T_{A2}a_0 \tag{6.6}$$

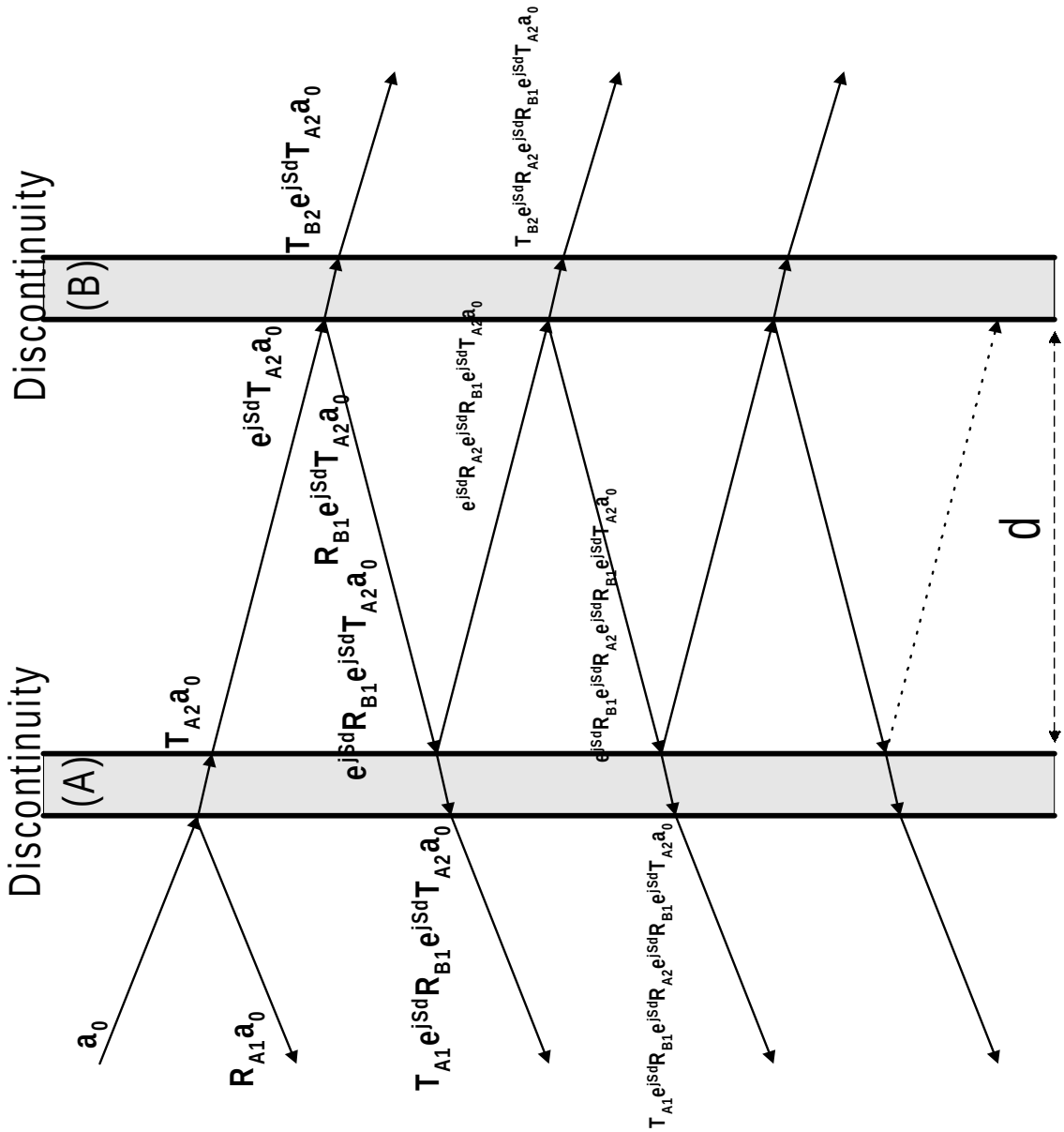

Figure 6.3: Multiple Reflections from two Cascaded Discontinuities

$$T_{02} = T_{B2}\left[\sum_{n=0}^{\infty}\left(e^{jSd}R_{A1}e^{jSd}R_{B1}\right)^{n}\right]e^{jSd}T_{A2} \quad (6.7)$$

$$T_{02} = T_{B2}\left(I - e^{jSd}R_{A2}e^{jSd}R_{B1}\right)^{-1}e^{jSd}T_{A2} \quad (6.8)$$

The quotients appearing in equations 6.4 and 6.8 are different. In order to make the computation of R_{01} and T_{02} more efficient, equation 6.1 is modified such that these quotient terms become identical. That is:

$$R_{01}a_0 = R_{A1}a_0 + T_{A1}e^{jSd}R_{B1}e^{jSd}T_{A2}a_0 + T_{A1}e^{jSd}R_{B1}\left(e^{jSd}R_{A2}e^{jSd}R_{B1}\right)e^{jSd}T_{A2}a_0 +$$

$$T_{A1}e^{jSd}R_{B1}(e^{jSd}R_{A2}e^{jSd}R_{B1}e^{jSd}R_{A2}e^{jSd}R_{B1})e^{jSd}T_{A2}a_0 + ... \quad (6.9)$$

$$R_{01} = R_{A1} + T_{A1}e^{jSd}R_{B1}\left[\sum_{n=0}^{\infty}\left(e^{jSd}R_{A2}e^{jSd}R_{B1}\right)^{n}\right]e^{jSd}T_{A2}a_0 \quad (6.10)$$

$$R_{01} = R_{A1} + T_{A1}e^{jSd}R_{B1}\left(I - e^{jSd}R_{A2}e^{jSd}R_{B1}\right)^{-1}e^{jSd}T_{A2} \quad (6.11)$$

Thus equations 6.8 and 6.11 are very similar to each other with a common quotient factor $\left(I - e^{jSd}R_{A2}e^{jSd}R_{B1}\right)^{-1}e^{jSd}T_{A2}$. This is the Cascading Algorithm which gives net reflection and transmission matrices of a cascaded structure composed of two sub-structures in terms of their individual reflection and transmission matrices.

6.4.1 Symmetrical and Periodic Structures

For symmetric discontinuities, A and B, $R_1 = R_2 = R$ and $T_1 = T_2 = T$. Thus equations 6.8 and 6.11 reduce to :

$$R_{01} = R_A + T_Ae^{jSd}R_B\left(I - e^{jSd}R_Ae^{jSd}R_B\right)^{-1}e^{jSd}T_A \quad (6.12)$$

$$T_{02} = T_B\left(I - e^{jSd}R_Ae^{jSd}R_B\right)^{-1}e^{jSd}T_A \quad (6.13)$$

If structures 'A' and 'B' are identical and symmetric, then $R_A = R_B$ and $T_A = T_B$. So the relations are further simplified to:

$$R_{01} = R + Te^{jSd}R\left(I - e^{jSd}Re^{jSd}R\right)^{-1}e^{jSd}T \tag{6.14}$$

$$T_{02} = T\left(I - e^{jSd}Re^{jSd}R\right)^{-1}e^{jSd}T \tag{6.15}$$

In addition, if the two identical and symmetric structures are connected to each other directly, such that $d = 0$, then:

$$R_{01} = R + TR\left(I - R^2\right)^{-1}T \tag{6.16}$$

$$T_{02} = T\left(I - R^2\right)^{-1}T \tag{6.17}$$

It is important to note that R_{01} and T_{02} are reflection and transmission matrices as seen from the left-hand side of the waveguide. The relations for R_{02} and T_{01} as seen from the right-hand side are easily obtained from 6.8 and 6.11 by interchanging $A \rightleftharpoons B$ and $1 \rightleftharpoons 2$. That is:

$$R_{02} = R_{B2} + T_{B2}e^{jSd}R_{A2}\left(I - e^{jSd}R_{B1}e^{jSd}R_{A2}\right)^{-1}e^{jSd}T_{B1} \tag{6.18}$$

$$T_{01} = T_{A1}\left(I - e^{jSd}R_{B1}e^{jSd}R_{A2}\right)^{-1}e^{jSd}T_{B1} \tag{6.19}$$

6.4.2 Rectangular Gratings

The rectangular grating is a classic example of a symmetrical periodic structure. With reference to figure 6.4, this problem can be solved by first considering the

discontinuity shown in figure 6.5. The reflection matrix for the TM polarized field in this case is given by:

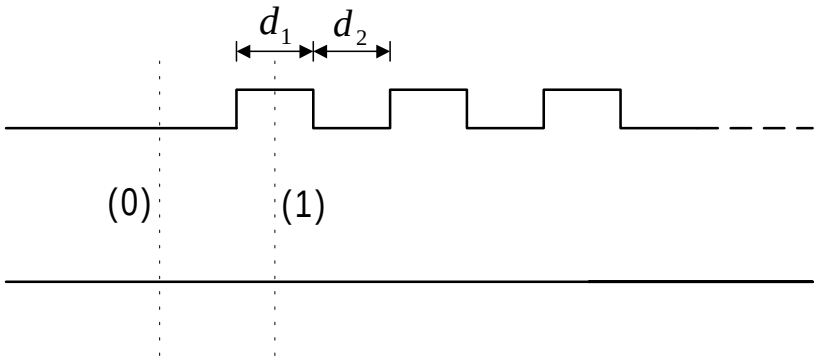

Figure 6.4: A Rectangular Waveguide Grating

$$R_{A1} = \left[I - S_0^{-1}N_0N_1^{-1}S_1\right]\left[I + S_0^{-1}N_0N_1^{-1}S_1\right]^{-1} \tag{6.20}$$

$$= \left[\left(S_0^{-1}N_0N_1^{-1}S_1\right)^{-1} - I\right] S_0^{-1}N_0N_1^{-1}S_1 \cdot \cdot \left[\left(\left(S_0^{-1}N_0N_1^{-1}S_1\right)^{-1} + I\right) S_0^{-1}N_0N_1^{-1}S_1\right]^{-1} \tag{6.21}$$

$$= \left[\left(S_0^{-1}N_0N_1^{-1}S_1\right)^{-1} - I\right] S_0^{-1}N_0N_1^{-1}S_1 \cdot \cdot \left(S_0^{-1}N_0N_1^{-1}S_1\right)^{-1}\left[\left(S_0^{-1}N_0N_1^{-1}S_1\right)^{-1} + I\right]^{-1} \tag{6.22}$$

$$= \left[\left(S_0^{-1}N_0N_1^{-1}S_1\right)^{-1} - I\right]\left[\left(S_0^{-1}N_0N_1^{-1}S_1\right)^{-1} + I\right]^{-1} \tag{6.23}$$

$$= -\left[I - \left(S_0^{-1}N_0N_1^{-1}S_1\right)^{-1}\right]\left[I + \left(S_0^{-1}N_0N_1^{-1}S_1\right)^{-1}\right]^{-1} \tag{6.24}$$

$$= -\left[I - S_1^{-1}N_1N_0^{-1}S_0\right]\left[I + S_1^{-1}N_1N_0^{-1}S_0\right]^{-1} \tag{6.25}$$

$$= -R_{A2} \tag{6.26}$$

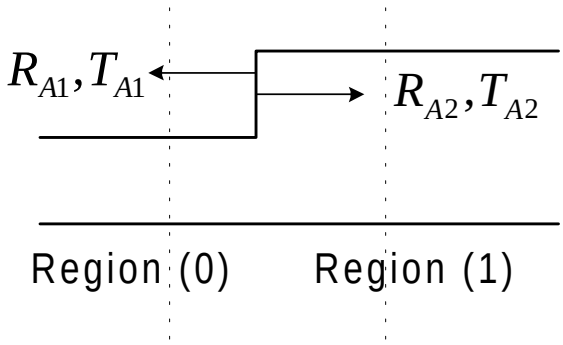

Figure 6.5: A Single Step Discontinuity

Thus for the above case $R_{A1} = -R_{A2}$, $T_{A2} = I + R_{A1}$ and $T_{A1} = I + R_{A2}$. Although these results were derived for the TM case, they also apply for the TE case as well. The next step is to treat the double discontinuity shown in figure 6.6. All Rs and Ts appearing in figure 6.6 can be expressed in terms of R_{A1}.

$$R_{A2} = -R_{A1} \tag{6.27}$$

$$T_{A1} = I + R_{A2} = I - R_{A1} \tag{6.28}$$

$$T_{A2} = I + R_{A1} \tag{6.29}$$

$$R_{B1} = R_{A2} = -R_{A1} \tag{6.30}$$

$$R_{B2} = R_{A1} \tag{6.31}$$

$$T_{B1} = T_{A2} = I + R_{A1} \tag{6.32}$$

$$T_{B2} = T_{A1} = I - R_{A1} \tag{6.33}$$

Since the structure of figure 6.6 is symmetric, we need only to define R and T

for the structure. Using equations 6.8 and 6.11 we obtain:

$$R = R_{A1} + (I - R_{A1})\, e^{jS_1 d_1}\, (-R_{A1}) \left[I - \left(e^{jS_1 d_1} R_{A1} \right)^2 \right]^{-1} \cdot e^{jS_1 d_1}\, (I + R_{A1}) \tag{6.34}$$

$$T = (I - R_{A1}) \left[I - \left(e^{jS_1 d_1} R_{A1} \right)^2 \right]^{-1} e^{jS_1 d_1}\, (I + R_{A1}) \tag{6.35}$$

The final step is to model the whole periodic structure iteratively. We start by combining the two symmetric identical structures as shown in figure 6.7. Using equations 6.14 and 6.15, the new reflection and transmission matrices for the combined structure is expressed in terms of the old reflection and transmission matrices of the individual structure, using the iterative relation:

$${R_{new}}' \leftarrow {R_{old}}' + {T_{old}}' e^{jS_0 d_0} {R_{old}}' \left[I - \left(e^{jS_0 d_0} {R_{old}}' \right)^2 \right]^{-1} e^{jS_0 d_0} {T_{old}}' \tag{6.36}$$

$${T_{new}}' \leftarrow {T_{old}}' \left[I - \left(e^{jS_0 d_0} {R_{old}}' \right)^2 \right]^{-1} e^{jS_0 d_0} {T_{old}}' \tag{6.37}$$

From figure 6.8, the above equations can be further modified and leads to the following relations:

$$R_{new} \leftarrow R_{old} + T_{old} R_{old} \left[I - R_{old}^2 \right]^{-1} T_{old} \tag{6.38}$$

$$T_{new} \leftarrow T_{old} \left[I - R_{old}^2 \right]^{-1} T_{old} \tag{6.39}$$

Equation 6.38 and 6.39 can be obtained by multiplying equations 6.36 and 6.37

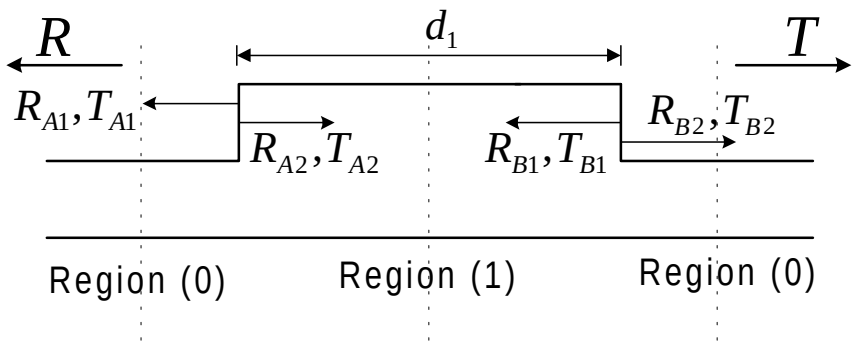

Figure 6.6: A Double Waveguide Discontinuity

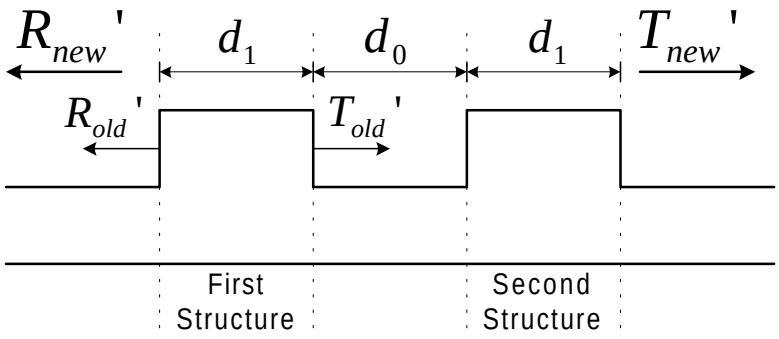

Figure 6.7: Two Identical Structures Cascaded with Separation d_0

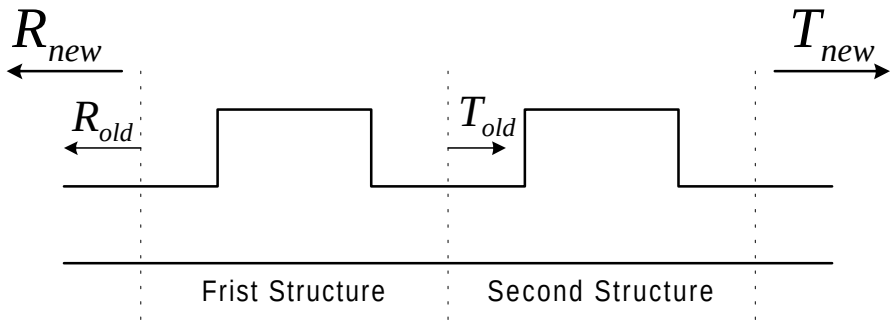

Figure 6.8: Two Identical Structures Cascaded Together

from the left by $e^{jS_0d_0}$ and defining the new quantities:

$$R_{old} = e^{jS_0d_0}R_{old}' \tag{6.40}$$

$$T_{old} = e^{jS_0d_0}T_{old}' \tag{6.41}$$

$$R_{new} = e^{jS_0d_0}R_{new}' \tag{6.42}$$

$$T_{new} = e^{jS_0d_0}T_{new}' \tag{6.43}$$

Equations 6.38 and 6.39 are the basis of the so called Doubling Algorithm. The factor $[I - R^2]^{-1}T$ is common in both equations which makes the algorithm very fast. At each iteration, the number of grating periods accounted for is doubled. That is after each iteration of equations 6.38 and 6.39 the number of periods accounted for is 2, 4, 8, 16, 32 and so on. This works in power of 2 only but we can model any number of periods by attaching the appropriate number of sections each having periods in power of 2. For example we can model 10 periods by attaching 8 and 2 periods. Note that the reflection and transmission matrices for 2 periods is already computed in the process of computing the reflection and transmission matrices of 8

periods. So these matrices are stored in a temporary location and later used in the attaching algorithm. For N discretization lines, this algorithm works on an $N \times N$ matrix for storage and eigen-value calculation. Some other algorithms [47, 64], based on raising a matrix to a certain power to model a certain number of periods, operate upon $2N \times 2N$ matrices. It becomes computationally expensive to find eigen-values and eigen-vectors of a $2N \times 2N$ matrix if the number of discretization lines N in a given problem space is large. So our algorithm has this extra advantage of modeling waveguides with wide (and hence large number N) cross-sections efficiently.

6.5 Results

In this section, the algorithm developed above is applied to calculate the spectral response of various waveguide gratings. As it will be seen later, the results obtained are in close agreement with published results, thus establishing the validity of this algorithm.

6.5.1 Air/GaAs/Air Waveguide Grating

A shallow waveguide grating having 256 periods as shown in the inset of figure 6.9 is modeled using a uniform mesh scheme. The TE_0 mode is launched in the waveguide and the reflected and transmitted fields are calculated. The fundamental-mode coefficient α_0 from the reflected field is calculated using an overlap integral (refer

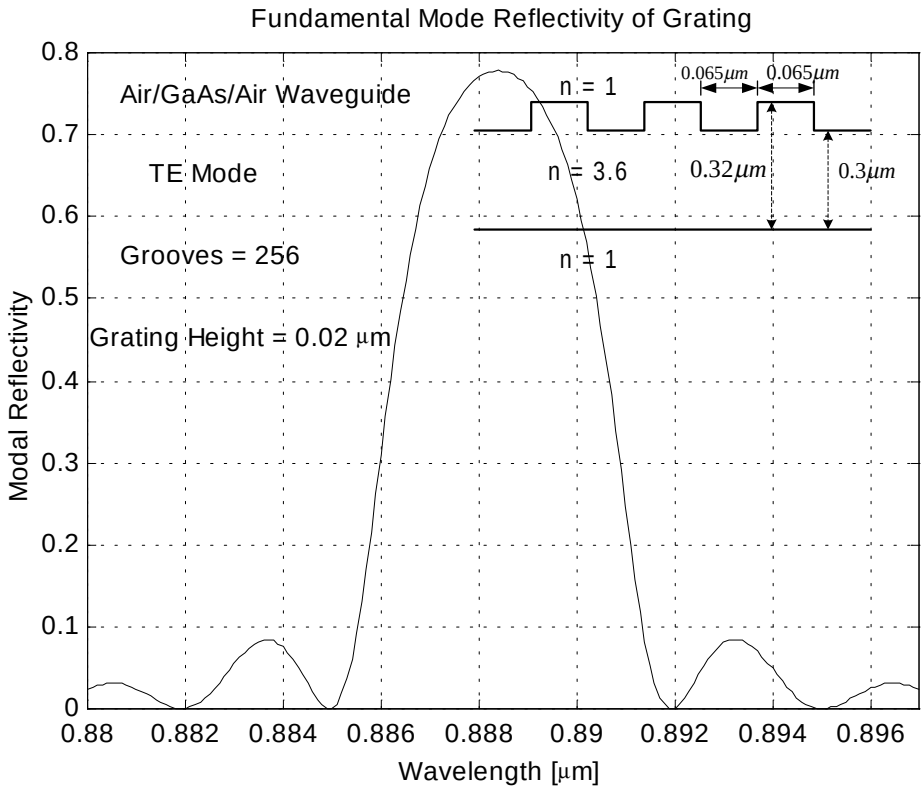

Figure 6.9: Modal Reflectivity of a Grating

to equation 5.19) and the modal reflectivity is plotted against the wavelength. As seen in figure 6.9, the modal reflectivity has a central main lobe and several side lobes. The calculation are done using a 5-point formulation. The number of sample points in the waveguide core layer is 15 and the width of cladding layers is chosen large enough (0.3 μm) to give a substantial evanescent field decay at the inner PML walls. A single layer PML is used with 7 sample points on each side of the computational window. The resulting absolute error in n_{eff} (Mol vs. Analytical) is 3.085e-5. The time required to simulate 256 periods at one wavelength is around 1.85 seconds (using an IBM Pentium III machine at 500 MHz with 128 MB RAM running MATLAB 5.2 under Windows 98).

6.5.2 Comparison with Published Results

An asymmetric waveguide with periodic deep grating (see figure 6.10) obtained from reference [86] is modeled using the Cascading and Doubling Algorithm introduced earlier. The modal spectral reflectivity is calculated for different number of periods. A non-uniform mesh with a single layer PML is used to model the device. The 5-point second-derivative approximation is used with appropriate interface conditions in the MOL . A total of 77 sample points are used in the problem space. As shown in figure 6.11, our results are in close agreement with those from [86], establishing the accuracy of our algorithm. As the number of periods is increased, the spectral reflectivity curve becomes asymmetric and the side lobes become more densely packed. Results for a grating with 262114 grooves (effectively semi-infinite) is given in figure 6.15 showing that the algorithm is stable for long gratings having several thousands of periods. It took approximately 5.5 seconds per wavelength to calculate the reflectivity and transmissivity of this semi-infinite case. The relative ease of the Doubling Algorithm to model long gratings is also evident due to the fact that, the number of periods modeled is doubled. The results for the TM polarization are also shown in figures 6.16 and 6.17 for 8192 and 16384 grating periods respectively. These results are quite different from the TE results in terms of the main lobe width and peak reflectivity. The peak reflectivity in the TM case has increased as compared to the TE case and the width of the main lobe has almost doubled.

In another simulation of the same device, the groove depth is reduced consider-

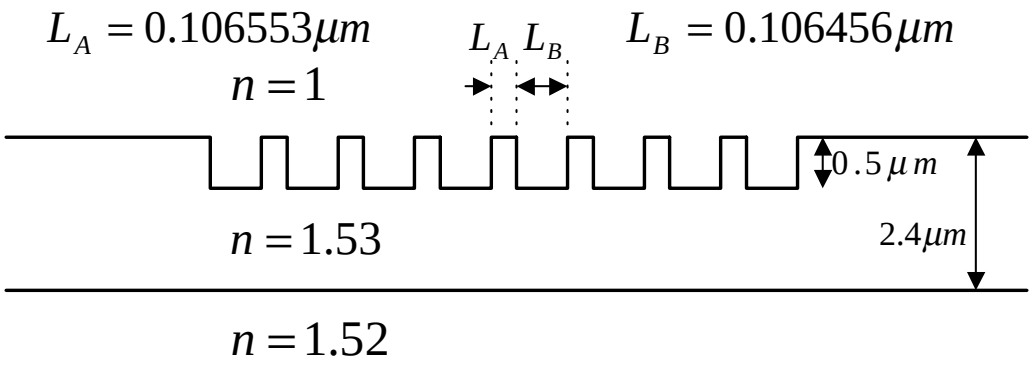

Figure 6.10: A Deep Waveguide Grating Structure

ably and the spectral response recalculated. In figure 6.18, the groove depth used is 0.42% with 65536 periods. The result shows that the main lobe width and side lobe level depend on the groove depth. For shallow gratings, the main lobe width is small and the side lobes are low, while for deep grating, the main lobe is wide and asymmetric with higher side lobe levels. The peak reflectivity becomes lower for the shallow grating. In this case, we need to use a larger number of grating periods to obtain a higher reflectivity at the resonance wavelength.

6.5.3 Effect of Changing the Groove Depth

A waveguide grating with 256 periods as shown in the inset of figure 6.21 is modeled. The spectral reflectivity of the TE_0 mode is calculated for different groove depths. The spectral responses for 10%, 20% and 30% grating depths are calculated and plotted in figures 6.21, 6.19 and 6.20 respectively. As the grating depth is increased,

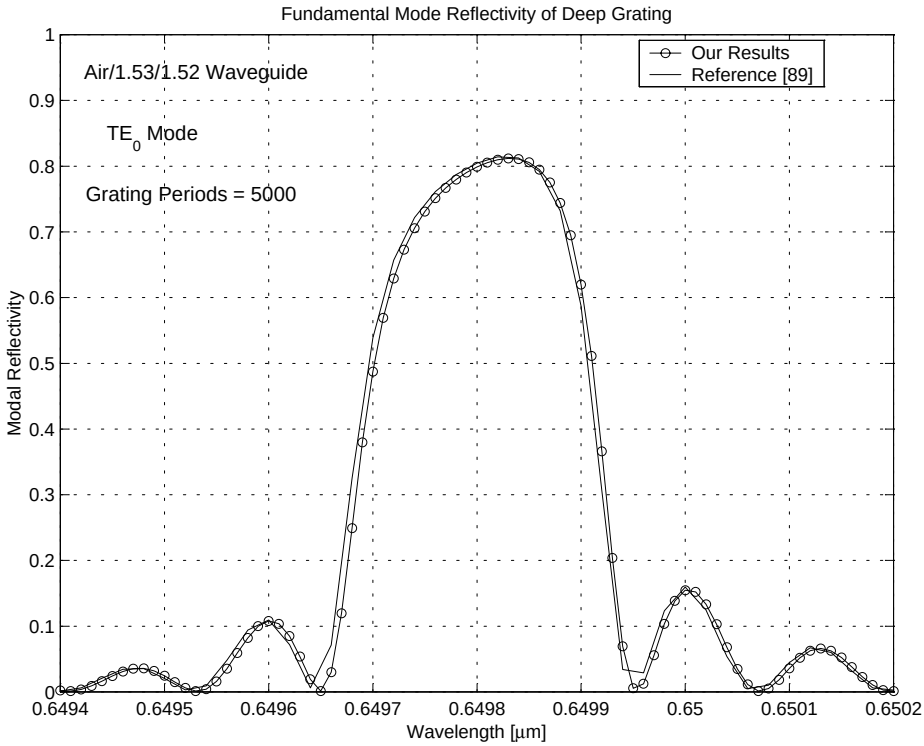

Figure 6.11: Deep Grating Modal Reflectivity

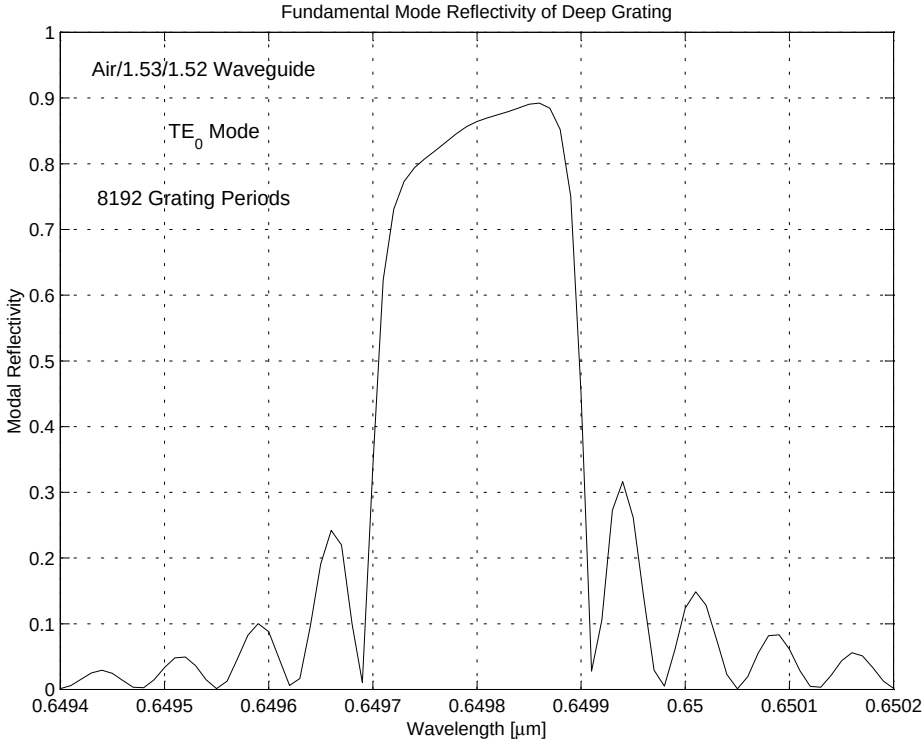

Figure 6.12: Deep Grating Modal Reflectivity, 8192 Periods

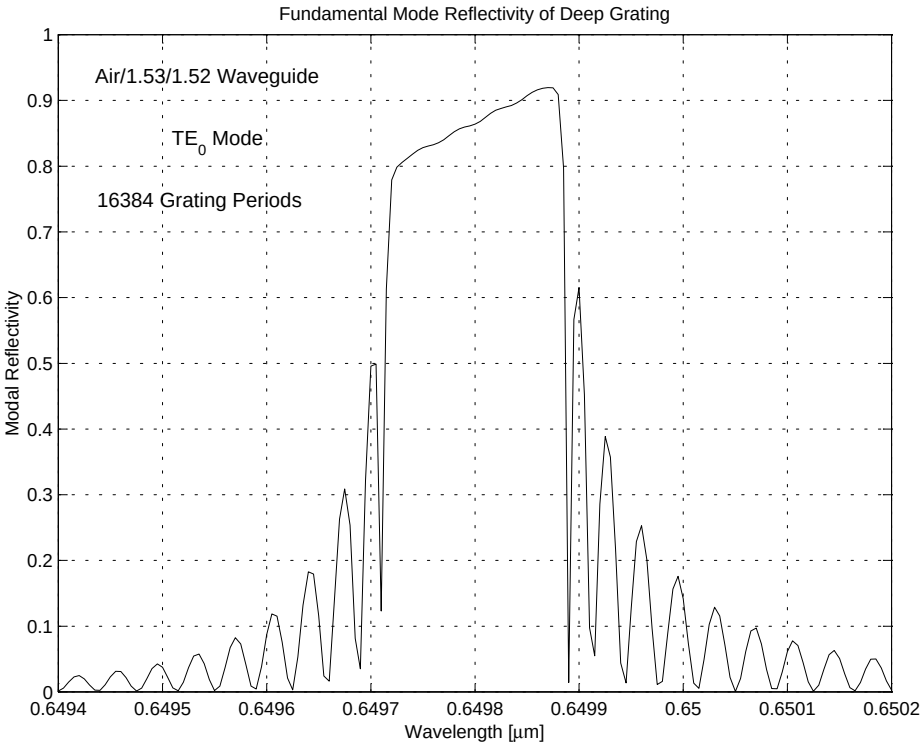

Figure 6.13: Deep Grating Modal Reflectivity, 16384 Periods

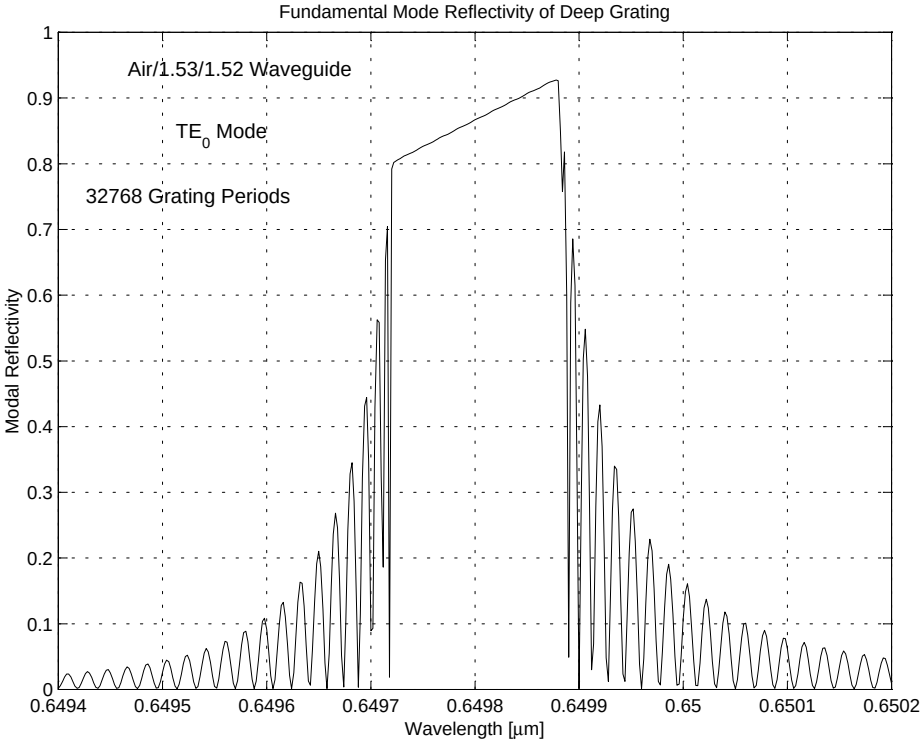

Figure 6.14: Deep Grating Modal Reflectivity, 32768 periods

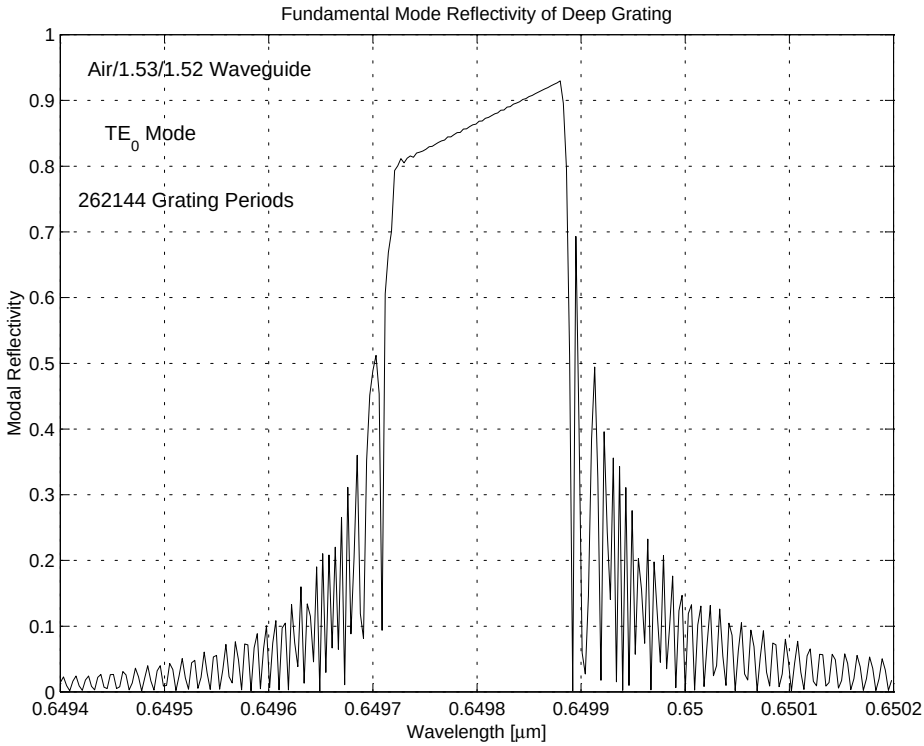

Figure 6.15: Deep Grating Modal Reflectivity, Semi-Infinite

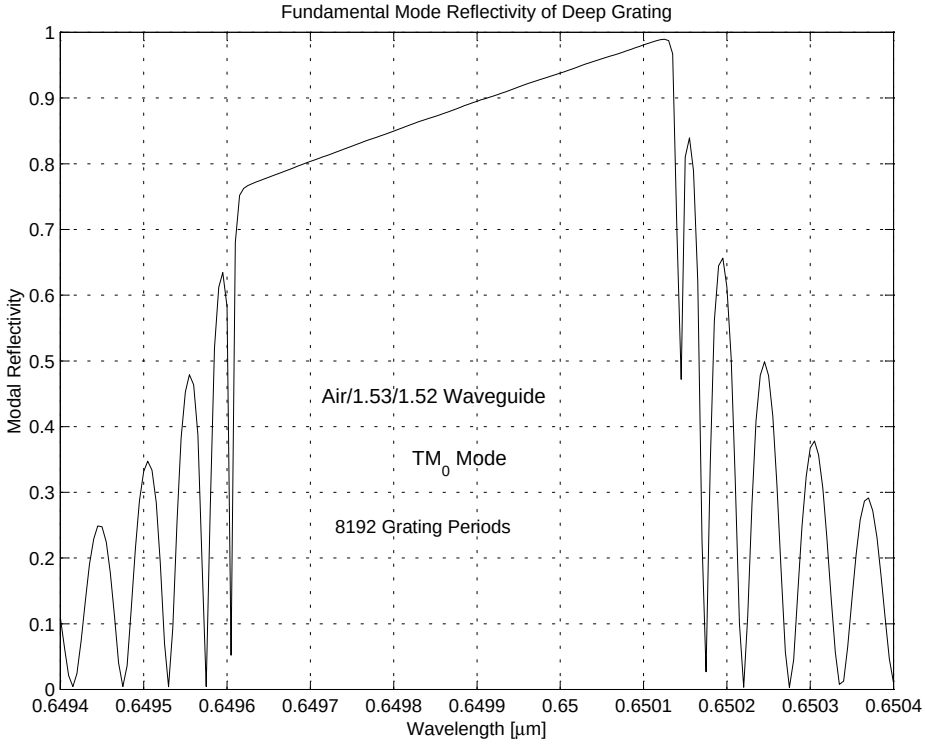

Figure 6.16: Deep Grating TM Modal Reflectivity, 8192 Periods

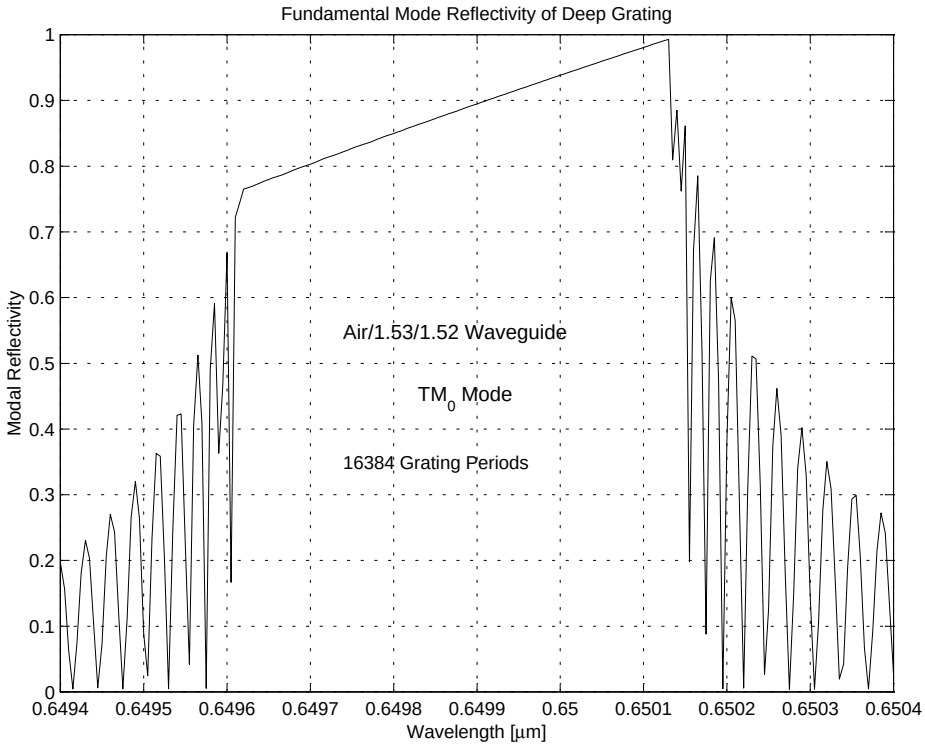

Figure 6.17: Deep Grating TM Modal Reflectivity, 16384 Periods

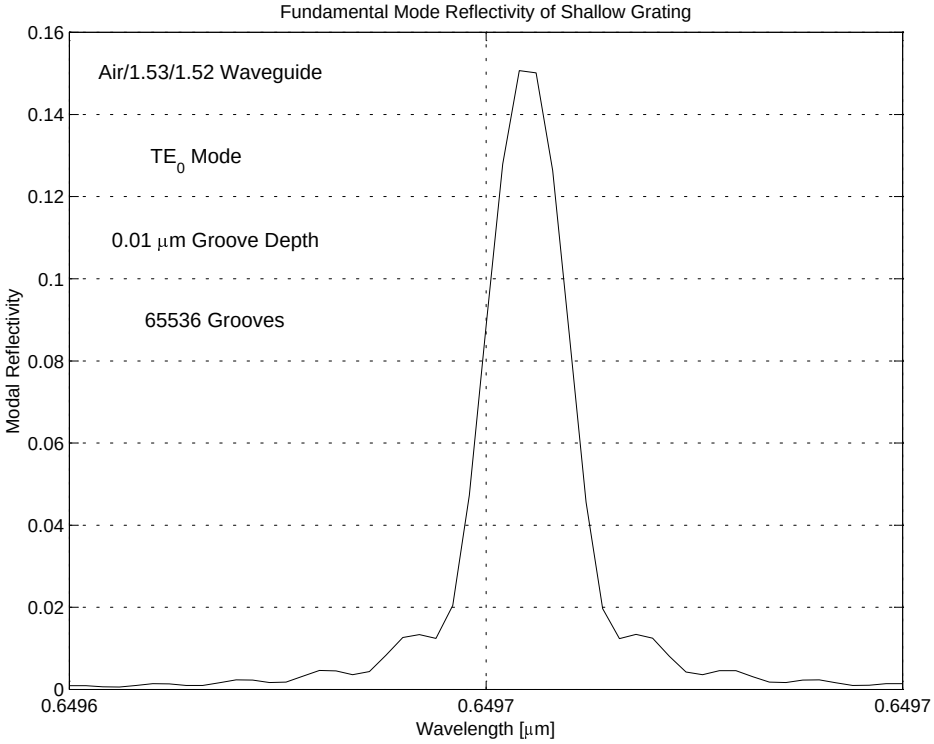

Figure 6.18: Modal Reflectivity of a Shallow Grating

the main lobe becomes wider and more asymmetric. The wavelength of peak reflectivity, often called the Bragg Wavelength λ_B shifts towards the shorter wavelength and the side lobe level increases.

6.6 Discussion

In this chapter, the cascading and doubling algorithm is used to model long gratings with a large number of grating periods. This algorithm is found to be fast and stable and its accuracy is verified against published results. This algorithm along with the MOL will be used to analyze the reflection mode polarizer in the next chapter.

It is concluded that the spectral reflectivity becomes asymmetric and the side lobes become more densely packed with the increase in the number of grating periods. The main lobe width and side lobe level depend on the groove depth and main lobe width and side lobe level increase with the groove depth.

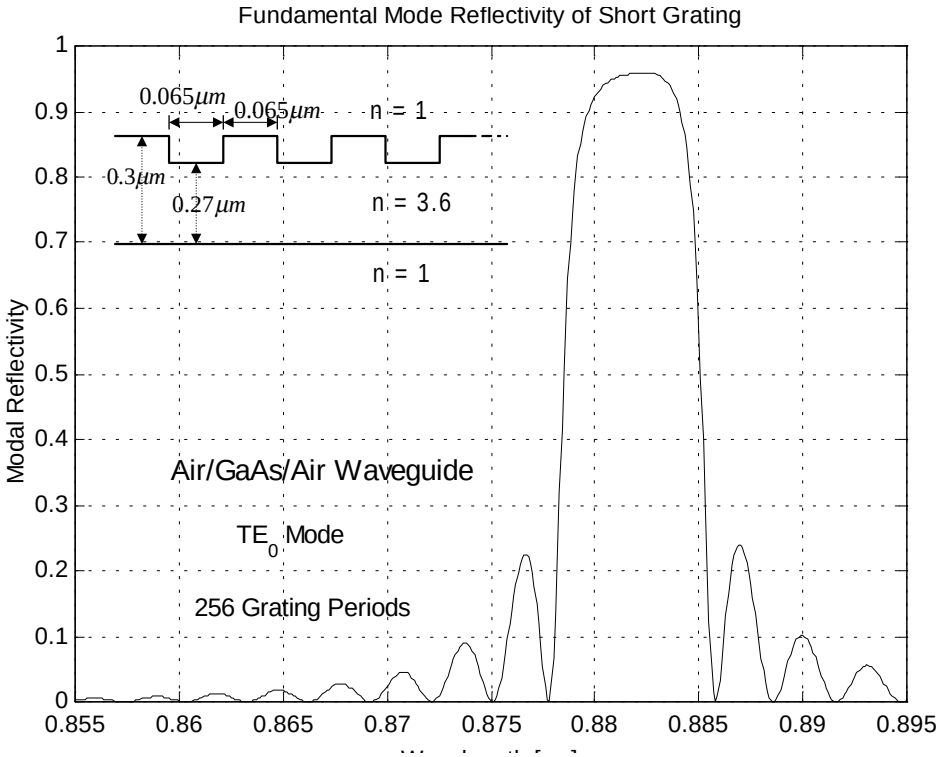

Figure 6.19: Short Grating Modal Reflectivity, 10% Grating Depth

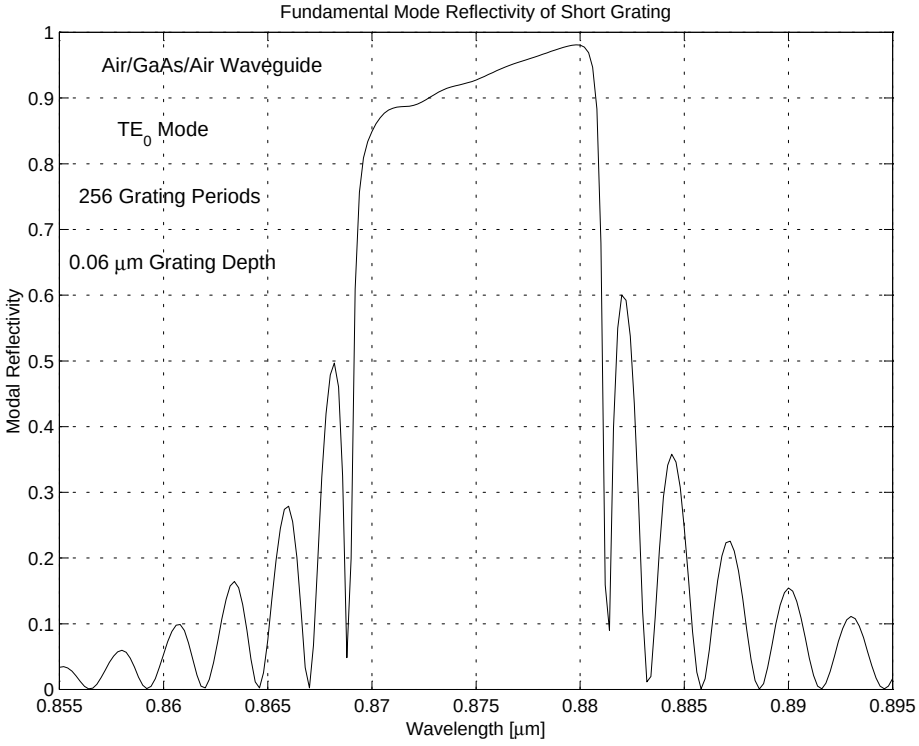

Figure 6.20: Short Grating Modal Reflectivity, 20% Grating Depth

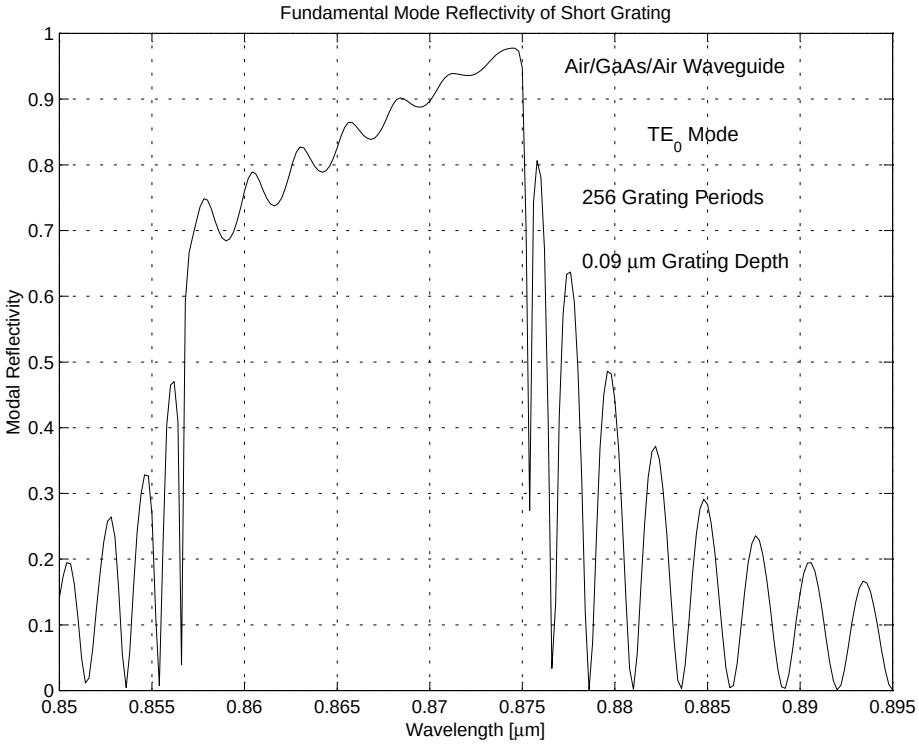

Figure 6.21: Short Grating Modal Reflectivity, 30% Grating Depth